Nanomaterial Biointerfacing *via* Mitochondrial Membrane Coating for Targeted Detoxification and Molecular Detection

Hua Gong, Qiangzhe Zhang, Anvita Komarla, Shuyan Wang, Yaou Duan, Zhidong Zhou, Fang Chen, Ronnie H. Fang, Sheng Xu, Weiwei Gao*, Liangfang Zhang*

Department of NanoEngineering, Chemical Engineering Program, Moores Cancer Center, University of California San Diego, La Jolla, CA 92093

*Corresponding authors: w5gao@ucsd.edu and zhang@ucsd.edu

Abstract

Natural cell membranes derived from various cell sources have been successfully utilized to coat nanomaterials for functionalization. However, intracellular membranes from the organelles of eukaryotes remain unexplored. Herein, we choose mitochondrion as a representative cell organelle and coat outer mitochondrial membrane (OMM) from mouse livers onto nanoparticles and field-effect transistors (FETs) through a membrane vesicle-substrate fusion process. Polymeric nanoparticles coated with OMM (OMM-NPs) can bind with ABT-263, a B-cell lymphoma protein 2 (Bcl-2) inhibitor that targets the OMM. As a result, OMM-NPs effectively protect the cells from ABT-263 induced cell death and apoptosis *in vitro* and attenuated ABT-263-induced thrombocytopenia *in vivo*. Meanwhile, FET sensors coated with OMM (OMM-FETs) can detect and distinguish anti-Bcl-2 antibody and small molecule agonists. Overall, these results show that OMM can be coated onto the surfaces of both nanoparticles and functional devices, suggesting that intracellular membranes can be used as coating materials for novel biointerfacing.

Keywords: Cell membrane coating, intracellular membrane, mitochondrion, detoxification, biosensor

Introduction

In the past few years, natural cell membranes have been increasingly used to coat synthetic nanomaterials for functionalization. A few advantages make this approach especially attractive. For example, its 'top-down' process skips molecular identification, providing nanomaterials with cell-like functions otherwise impractical to replicate using traditional synthesis.²⁻³ The membrane coating also provides synthetic substrates with an array of cellspecific proteins that can be leveraged for dynamic and multiplex binding interactions, resulting in function-driven and broad-spectrum bioactivity. 4-5 When cell membranes are coated onto a solid substrate, they can bind toxins and sequester their toxicity while preserving native toxin structures desirable for effective immune processing.⁶⁻⁷ Additionally, molecular binding to the cell membrane causes electronic perturbation that can be captured and measured through devices on the substrate, enabling sensitive and quantitative detection of biological compounds. 8 With these advantages, the cell membrane coating technology, initially developed with red blood cell membrane, 9-14 has expanded to using the membranes from various cell types, including platelets, cancer cells, immune cells, stem cells, and epithelial cells. 9-14 Membranes of extracellular vesicles released from mammalian cells and bacteria have also been collected for coating due to their distinct antigenic profile or tissue adhesion properties. 15-17 With multifaceted biointerfacing with complex biological systems, cell membrane-coated nanomaterials have enabled a wide range of applications in drug delivery, detoxification, immune modulation, and biosensing. 1, 18

Despite its rapid development, the cell membrane coating technology has been focused primarily on using the plasma membranes that separate the interior of a cell from its outside environment for coating. To harness a broader range of functionalities, one would wonder whether intracellular membranes, which encapsulate subcellular structures or organelles inside a

eukaryotic cell, can also be used for coating. Intracellular membranes share the same fundamental structure as the plasma membranes, where the phospholipid bilayer forms a stable barrier embedded with proteins to carry out the specific functions of each cell organelle. 19-20 Targeting intracellular membrane functions underlies a variety of therapeutic strategies. For example, the delivery of macromolecules across the nuclear membranes is a key step toward safe and effective gene therapy. 21-22 In cancer treatment, targeting the permeabilization of the nuclear, mitochondrial, or lysosomal membranes is a popular strategy to bypass anticancer drug resistance of the downstream pathways. 23-24 To counteract drug-resistant bacterial or viral infections, blocking the alteration of intracellular membranes by the pathogens is crucial to inhibit their intracellular replication. 25-26 Apparently, coating intracellular membranes onto synthetic nanomaterials, if successful, would hold great promise to probe complex intracellular machinery and open new therapeutic opportunities.

To investigate intracellular membrane coating, in this study we selected mitochondrion as a model cell organelle and investigated the coating of outer mitochondrial membrane (OMM) onto synthetic nanomaterials. The mitochondria are a key cell organelle responsible for producing adenosine triphosphate, maintaining redox homeostasis, and controlling cell apoptosis. We isolated and purified OMM and coated it onto synthetic substrates, including polymeric nanoparticles and field-effect transistors (FETs), respectively (**Figure 1**). Nanoparticles coated with OMM (denoted 'OMM-NPs') inherited OMM-specific surface antigens, which were able to bind OMM ligands and neutralize their toxicity both *in vitro* and *in vivo*. Meanwhile, carbon nanotube-based FETs coated with OMM (denoted 'OMM-FETs') also showed selective interaction with OMM ligands and detected them in correlation with their binding affinity to the OMM. In this study, through successful OMM coating and biointerfacing, we demonstrated the

feasibility of using intracellular membranes to coat synthetic nanomaterials. This approach may lead to new functional nanomaterials or nanodevices for disease treatment and diagnosis.

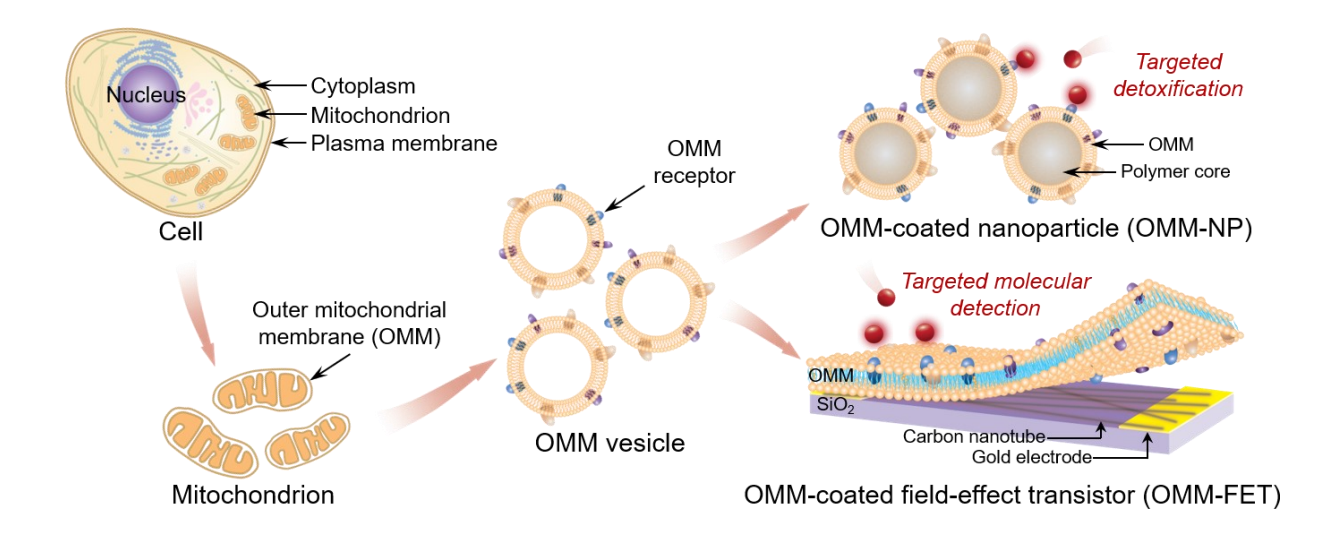


Figure 1. A schematic illustration of coating outer mitochondrial membrane (OMM) for targeted detoxification and molecular detection. Briefly, mitochondria are first collected from source cells and then the OMM is isolated and purified. With a sonication method, OMM vesicles are prepared and fused with polymeric nanoparticle cores or carbon nanotube-based field-effect transistors (FETs), translocating the entire OMM and the associated protein receptors onto the synthetic substrates. The OMM-coated nanoparticles (denoted 'OMM-NPs') can bind to OMM-specific ligands towards detoxification and the OMM-coated FETs (denoted 'OMM-FETs') are capable for detecting OMM-specific molecules.

Results and Discussion

The fabrication of OMM-NPs was divided into three steps. In the first step, we collected mitochondria from mouse livers and purified them through sucrose density gradient centrifugation (Figure S1).²⁷ Then, the OMM was isolated by osmotic shock followed by density gradient centrifugation.²⁸ The purity of OMM was confirmed by analyzing the concentrations of cytochrome c (a marker of the intermembrane space), DNA (a marker of the mitochondrial

matrix), and B-cell lymphoma protein 2 (Bcl-2, a surface marker of OMM) (Figure S2). In the second step, we made polymeric cores of poly (lactic-co-glycolic acid) (PLGA) by using an established nanoprecipitation method. In the last step, we added the OMM to the PLGA core suspension at a membrane protein-to-polymer weight ratio of 1:1, followed by sonication to form the OMM-NPs (Figure S3). The OMM coating onto PLGA cores was monitored by changes in the core size and surface zeta potential before and after the sonication process. After the coating, the diameter of the PLGA cores increased from 103 ± 9.4 nm to 128 ± 15.3 nm (Figure 2A). Meanwhile, the surface zeta potential of PLGA cores also changed from -42.2 ± 1.3 mV to -25.0 ± 3.4 mV due to the charge screening by the OMM coating. To further confirm the OMM coating, the nanoparticles were stained with uranyl acetate and visualized by transmission electron microscopy (TEM). Under the TEM, all particles showed a spherical core-shell structure that reflected the enclosure of the PLGA core in a thin shell (Figure 2B). The thickness of the membrane shell is 9.0 ± 1.6 nm, consistent with 7.5 nm of the reported membrane thickness of the OMM. These results demonstrate the successful coating of the PLGA cores with the OMM.

Following the formulation, we examined the surface proteins of the OMM-NPs to verify the mitochondrial functionalization. First, the protein profiles of OMM lysate and OMM-NPs were analyzed with sodium dodecyl sulfate polyacrylamide gel electrophoresis (SDS-PAGE). As shown in Figure 2C, the protein profile of OMM-NPs matched well with that of the OMM lysate, indicating the preservation of membrane proteins on OMM-NPs throughout the fabrication process. In addition, a western blotting analysis showed the presence of Bcl-2 in samples of mitochondria, OMM, and OMM-NPs (Figure 2D). Significant enrichment of Bcl-2 was observed in OMM and OMM-NPs, further confirming the translocation of OMM and associated membrane proteins onto the nanoparticle surface. To examine the membrane orientation, we

stained the mitochondria and OMM-NPs that contained equal amounts of membrane content with fluorescence-labeled anti-Bcl-2 antibody. After removing the free antibodies, the OMM-NP sample showed a comparable fluorescence intensity with that of the mitochondrial sample (Figure 2E). An inside-out membrane coating would likely block antibody staining and reduce fluorescence intensity. Therefore, a comparable fluorescence intensity between OMM-NPs and mitochondria suggests that OMM-NPs adopted a right-side-out membrane orientation. The asymmetric charge across the membrane determines the right-side-out orientation during the coating process, which is vital for the OMM functions. 31-32 Moreover, the resulting OMM-NPs were stable in water, 1X PBS, and 50% serum. No detectable increase in nanoparticle size was observed over 48 h (Figure 2F).

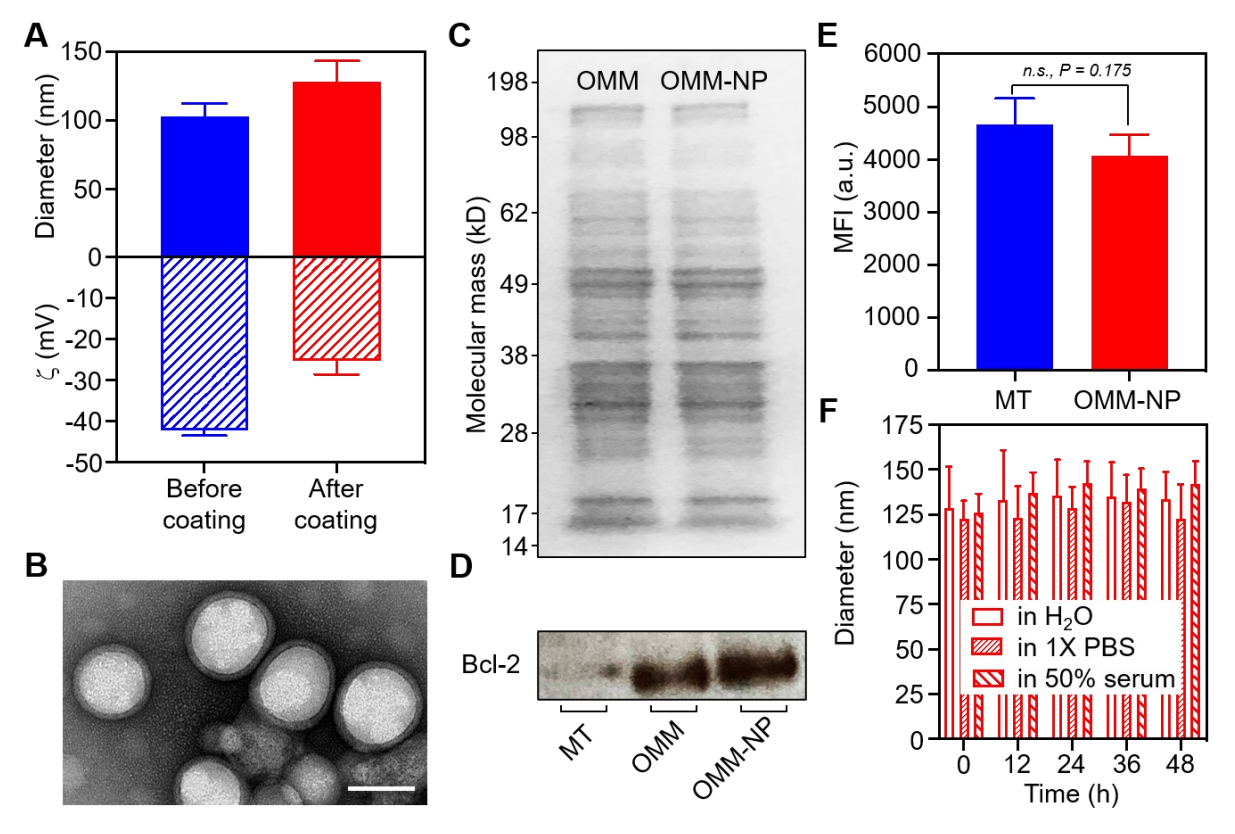


Figure 2. Characterization of OMM-NPs. (A) Dynamic light scattering measurements of hydrodynamic size (diameter, nm) and surface zeta-potential (ζ , mV) of OMM-NPs before and after coating with OMMs (n = 3, mean + standard deviation). (B) TEM images of OMM-NPs

negatively stained with uranyl acetate. (Scale bar = 100 nm.) (C) SDS-PAGE protein analysis of OMMs and OMM-NPs. Samples were run at equivalent protein concentrations and stained with Coomassie Blue. (D) Western blot analysis showing the Bcl-2 expression on whole mitochondria (MT), OMMs, and OMM-NPs, respectively. (E) Comparison of the fluorescence intensity measured from MT (100 μ L, ~16 mg/mL MT) or OMM-NPs (100 μ L, 1.2 mg/mL protein concentration) containing equal amounts of membrane content and stained with 1 μ L of Alexa Fluor 647 labeled anti-Bcl-2 antibodies. Error bars represent standard deviations (n=3, mean + standard deviation, *n.s.*: not significant). Statistical analysis was performed by using two-tail Student's *t*-test. (F) Stability of OMM-NPs in water, 1X PBS, and 50% serum, determined by monitoring the nanoparticle size (diameter, nm) as a function of incubation time over 48 h (n = 3, mean + standard deviation).

We next investigated the binding capacity of OMM-NPs with ABT-263 (MW = 974.6 g/mol), a cytotoxic ligand of Bcl-2 that induces cell apoptosis. ³³ To examine the dose-dependent binding of OMM-NPs with ABT-263 ligand, we mixed OMM-NPs at varying concentrations with ABT-263 at three fixed concentrations and then quantified the unbound ABT-263 in each experimental setting using high-performance liquid chromatography (HPLC). We calculated the bound ABT-263 by subtracting the measured unbound ABT-263 from the initial input of ABT-263. As shown in **Figure 3**A, the percent of bound ABT-263 with all three initial concentrations followed a sigmoidal curve as a function of the log of the OMM-NP concentrations. The effective concentrations of OMM-NPs that bound with 50% of the ABT-263 (defined as 'IC50') was 0.30 ± 0.07 , 0.49 ± 0.12 , and 1.1 ± 0.05 mg/mL corresponding to ABT-263 initial concentrations of 0.3, 1, and 3 μ M, respectively. The effective concentrations of OMM-NPs that bound with 100% of the ABT-263 (defined as 'IC100') was 0.65 ± 0.06 , 1.5 ± 0.13 , and 2.5 ± 0.17 mg/mL for the same set of ABT-263 initial concentrations. Next, we evaluated the neutralization capacity of OMM-NPs against the cytotoxicity of ABT-263 on HL-60 cells, a

model monocyte-like cell line. As shown in Figure 2B, increasing the amount of free ABT-263 added to the cells resulted in decreased cell viability determined with an ATP assay. We then fixed the ABT-263 concentration at 2 μ M, the effective concentration that killed 50% of the cells (EC50), and varied OMM-NP concentrations from 0.03 to 2 mg/mL. ABT-263 is known to induce apoptosis by activating Caspase-3 and Caspase-7 pathways. OMM-NPs were able to block the caspase activation by ABT-263 (Figure S4). As the OMM-NP concentration increased, the cell viability increased accordingly (Figure 3C). The concentration of OMM-NPs that neutralized half of the ABT-263 cytotoxicity (IC50) was 0.65 ± 0.08 mg/mL, and OMM-NP at a concentration of approximately 1.2 ± 0.10 mg/mL (IC100) was needed to fully neutralize the cytotoxicity of ABT-263.

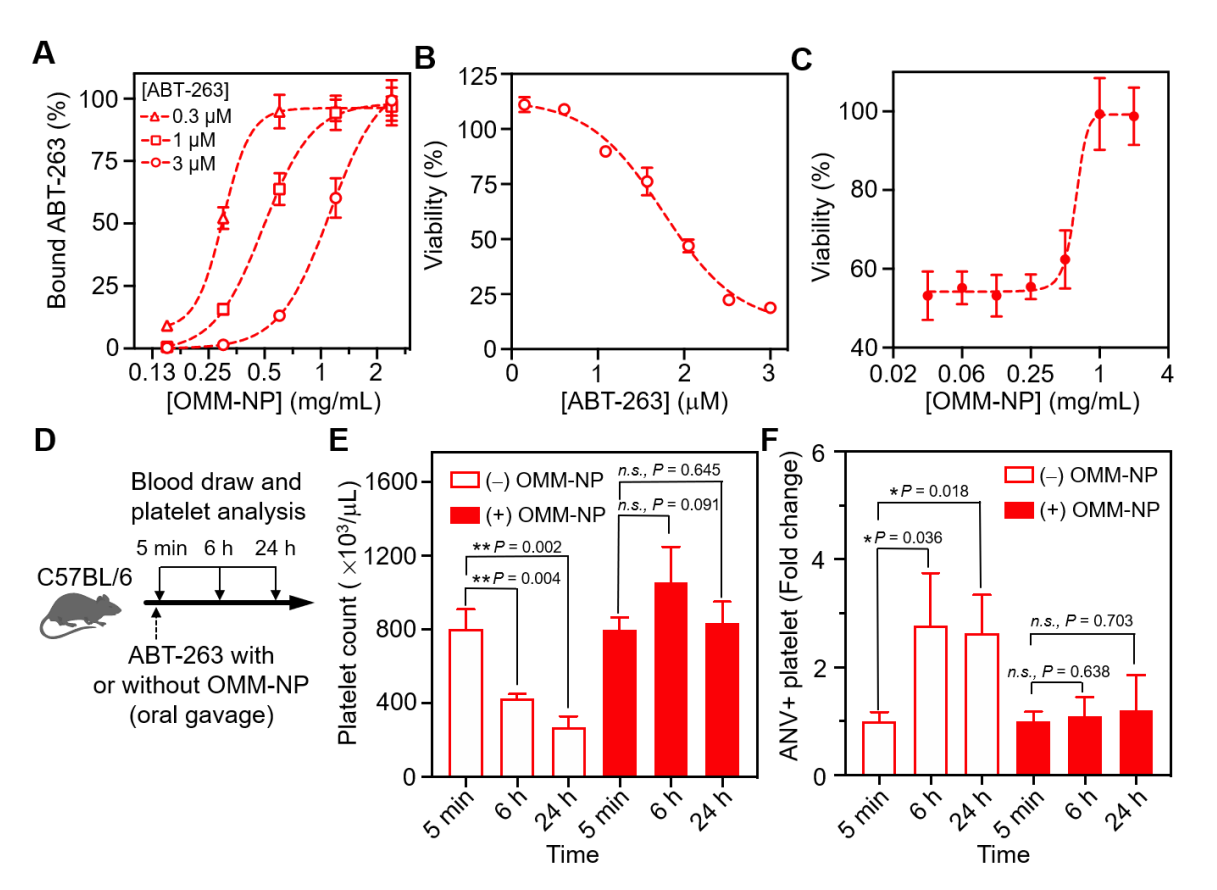


Figure 3. *In vitro* and *in vivo* detoxification by OMM-NPs. (A) Quantification of ABT-263 binding capacity of OMM-NPs. ABT-263 initial concentration was fixed at 3, 1, and 0.3 μM

while the concentration of OMM-NPs was varied from 0.13 to 2 mg/mL. (B) Viability of HL-60 cells treated with ABT-263 at various concentrations. (C) Dose-dependent ABT-263 neutralization with OMM-NPs against cytotoxicity on HL-60 cells. Neutralization was performed in a pre-incubation regimen, where OMM-NPs were mixed with ABT-263 and then the mixture was added to the cells. ABT-263 concentration was fixed at 2 mM while the concentrations of OMM-NPs were varied from 0.03 to 2 mg/mL. (In A-C, n = 3; mean \pm standard deviation.) (D) The study protocol of testing OMM-NP detoxification against ABT-263 toxicity *in vivo*. ABT-263 at a dosage of 1 mg/kg with or without OMM-NPs were injected into C57/BL6 mice (n = 3) through oral gavage. The platelet count and apoptosis were examined at 5 min, 6 h, and 24 h by flow cytometry. Alexa Fluor 647 labeled CD41 was selected as platelet marker while Annexin V (ANV) was used as an apoptosis marker. (E) Platelet counts after oral administration of ABT-263 or the mixture of ABT-263 and OMM-NPs. (F) Quantification of apoptotic platelets in the mouse blood. In E and F, n = 3 independent experiments using the same batch of OMM; mean + standard deviation. Statistical analysis was performed by using two-tail Student's t-test.

Thrombocytopenia is a major adverse effect associated with the clinical use of ABT-263.³⁷⁻³⁸ In the study, we tested the efficacy of OMM-NPs in neutralizing ABT-263-induced thrombocytopenia *in vivo*. Mice were administered through oral gavage with either ABT-263 at a dosage of 1 µmol/kg or the same dosage of ABT-263 but immediately followed by treating with OMM-NPs at a dosage of 800 mg/kg (Figure 3D). Blood was collected at 5 min, 6 h, and 24 h after the oral gavage. The analysis of the blood samples from mice administered with ABT-263 alone showed a continuous drop of platelet counted with flow cytometry by staining the blood with antimouse CD41-Alexa Fluor 647 (Figure 3E and Figure S5A). In contrast, platelet counts in samples from the mice administered with both ABT-263 and OMM-NPs remained at the baseline. In addition, residual circulating platelets from mice treated with ABT-263 without OMM-NPs showed an increase of the percentage of annexin V positive cells, indicating an increase of phosphatidylserine (PS) exposure due to ABT-263-induced apoptosis (Figure 3F and Figure S5B).

Despite the same dosage of ABT-263 in both groups, the increase of PS exposure was absent in platelets from mice administered with ABT-263 and OMM-NPs. The results clearly demonstrate the therapeutic efficacy of OMM-NPs in neutralizing toxic compound ABT-263 *in vivo*.

After having demonstrated OMM coating onto synthetic nanoparticles for targeted molecular binding and detoxification, we next examined the ability of OMM interfacing with nanodevices for molecular detection. In the study, we first made OMM vesicles and allowed them to fuse onto a p-type carbon nanotube-based FET spontaneously. The OMM fusion was tested by using OMM vesicles labeled with DiD dye, a lipophilic dye (1'-dioctadecyl-3,3,3',3'tetramethylindodicar-bocyanine, 4-chlorobenzenesulfonate salt, excitation/emission = 644/665 nm). After washing away the vesicle suspension, the fluorescence image of the device showed a strong signal from the labeled membrane with even distribution on the FET surface (Figure 4A). We also labeled OMM-NPs with DiD dye as a non-fusogenic control to test the fusion. After applying the same incubation and washing steps, we observed little fluorescence from the FET surface. The imaging result ruled out non-specific adsorption as a potential reason for the membrane retention on the FET surface. The fusion was further tested with dual-fluorescencelabeled OMM vesicles. One fluorescent dye (DiD) was incorporated into the bilayer membrane of the vesicles. The other (BSA-fluorescein, excitation/emission = 488/525 nm) was encapsulated inside the aqueous compartment of the vesicles. Following the same incubation process, only the fluorescence signal from the membrane was detected from the FET surface, indicating the loss of the inner content during the vesicle-FET fusion process (Figure 4B). These results indicate a successful coating of OMM onto the FET surfaces. We also tested the electrical property of OMM-FET and an uncoated FET to examine the effect of membrane fusion. In both tests, when the source-drain voltage $(V_{\rm ds})$ was fixed, the absolute value of the source-drain

current (I_{ds}) of the device decreased when the gate voltage (V_g) became less negative, suggesting the semiconductive properties of the FETs were well maintained after OMM coating (Figure 4C). In addition, under the same V_g and V_{ds} , the absolute values of I_{ds} measured from OMM-FETs were lower than those from the uncoated FETs, indicating an increase of resistance upon OMM coating (Figure S6).

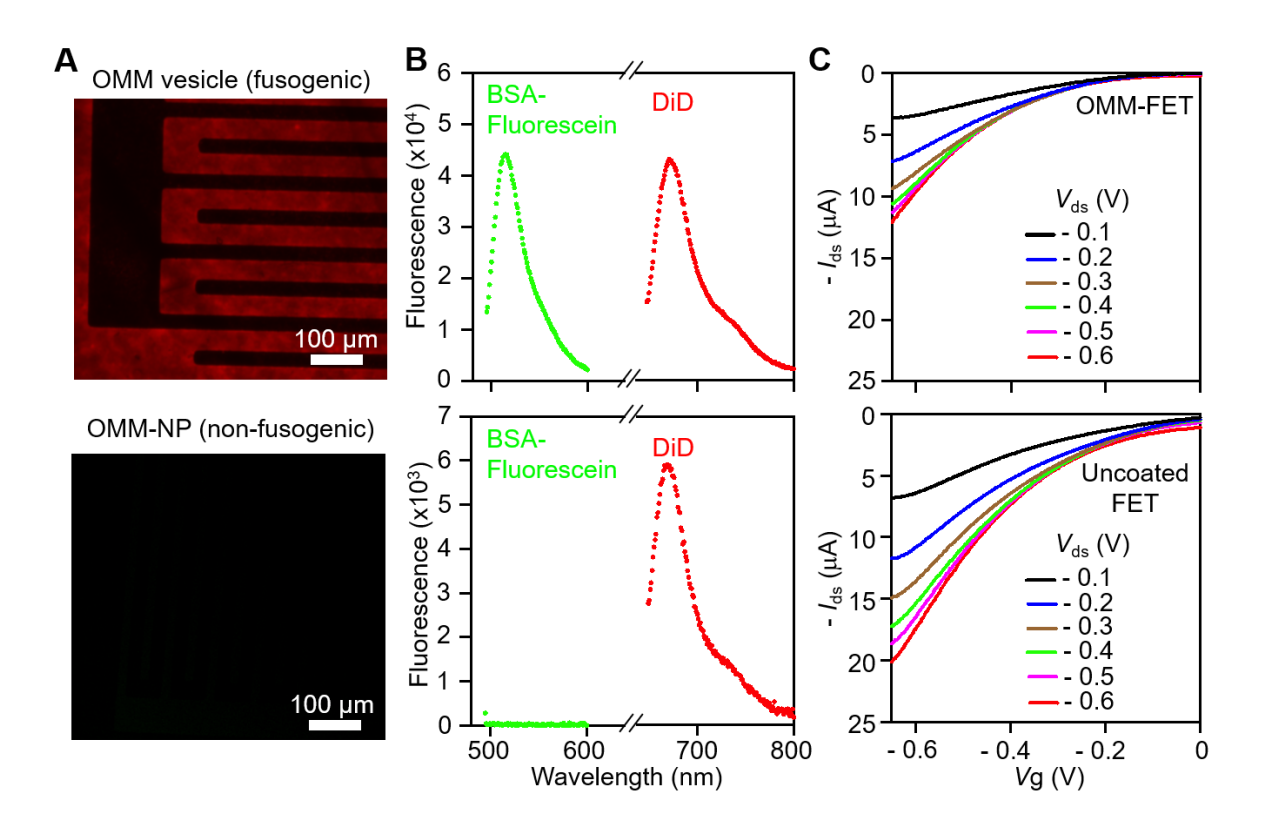


Figure 4. Characterization of OMM-FETs. (A) Fusogenic OMM vesicles (top panel) and non-fusogenic OMM-NPs (bottom panel), both labeled with DiD dye, were incubated with an FET substrate, respectively. The fluorescence images were taken after the incubation and the removal of the nanoparticle suspensions. (B) OMM vesicles were labeled with two fluorescent dyes: DiD (red) in the membrane and BSA-Fluorescein (green) in the aqueous compartment of the vesicles. Fluorescence emission spectra of the OMM vesicles before (top) and after (bottom) their incubation with the FET substrate were taken and compared. (C) To examine the semiconductive properties of OMM-FETs, the $I_{\rm ds}$ – $V_{\rm g}$ curves of an OMM-FET (top) and an uncoated FET (bottom) were measured. The $V_{\rm ds}$ values were varied from -0.6 V to -0.1 V.

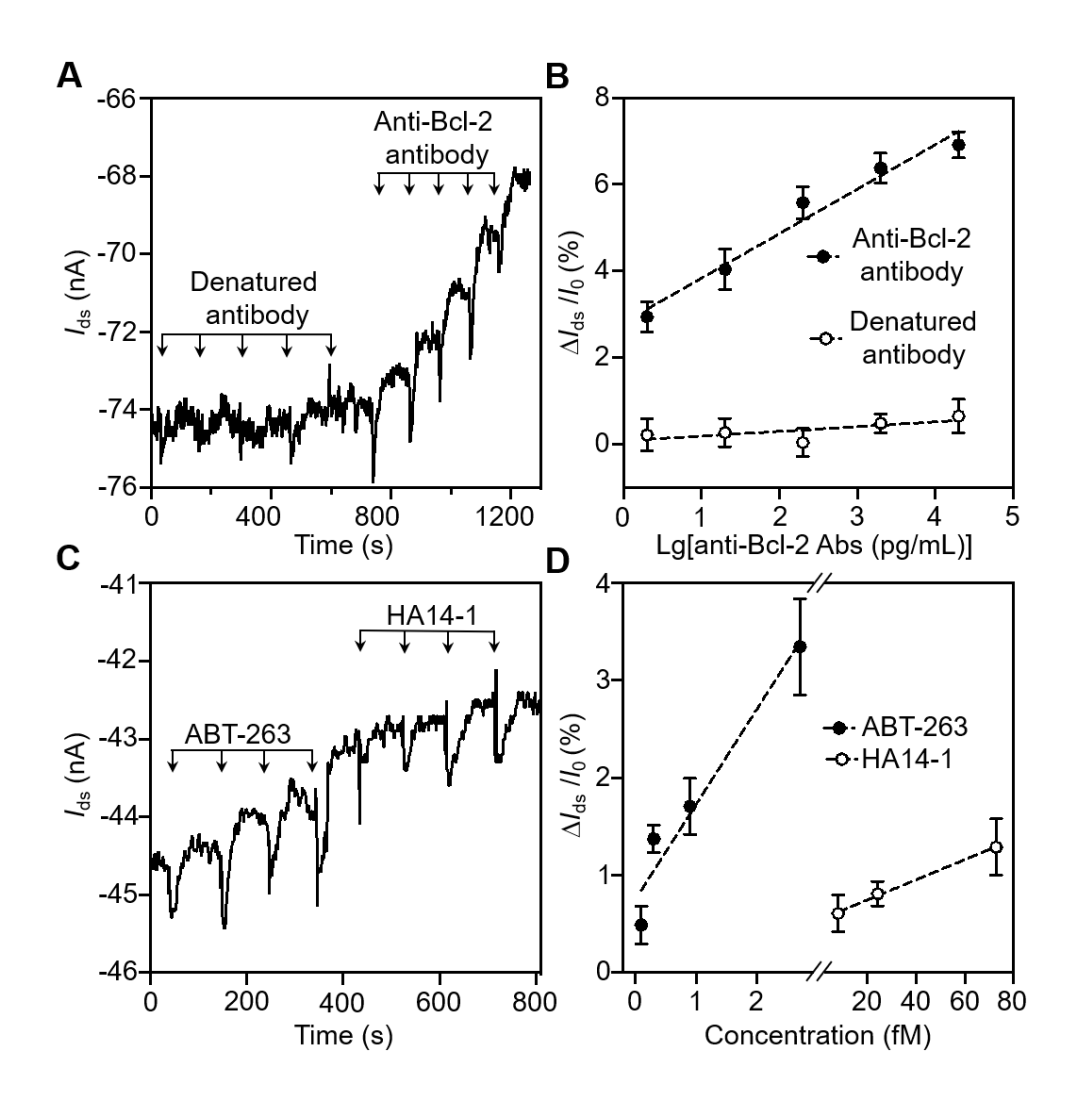


Figure 5. Detection of OMM-reactive compounds by OMM-FETs. (A, B) Anti-Bcl-2 antibodies and (C, D) ABT-263 and HA14-1, two small molecule Bcl-2 inhibitors, were used as model molecules for the test. OMM-FETs were used to measure the channel conductance as more antibodies and inhibitors were added to the OMM-FET surface. Typical I_{ds} —time curves of the compounds (A and C) were measured, and values of I_{ds} change relative to the basal level ($\Delta I_{ds}/I_0$) were plotted against compound concentrations (B and D). In B and D, the error bars were obtained by randomly picking 30 timepoints from the plateau of the I_{ds} - time curves after adding each molecule; mean \pm standard deviation.

Next, we examined the OMM-FETs for their ability to detect OMM-reactive biomolecules, including antibodies and small molecule compounds. We designed our study to

measure multiple molecules on a single device. For this purpose, we avoided device saturation by measuring molecules with low concentrations at the leading edge of the binding curves.^{8, 39-40} We first chose anti-Bcl-2 IgG antibody for the test. When we added denatured antibodies onto an OMM-FET, there were no changes of OMM-FET channel conductance after each addition (**Figure 5**A). However, when we added non-denatured anti-Bcl-2 antibodies onto the device, the absolute values of I_{ds} decreased stepwisely following discrete changes of the antibody concentrations. A decrease of channel conductance indicates that binding of the antibody molecules repels holes in the *p*-type OMM-FET.^{8, 41} Based on these measurements, we found linear correlations between the changes of the I_{ds} values and the antibody concentrations (Figure 5B). The difference between their slopes is significant, suggesting the ability of the OMM-FET to distinguish molecules with different binding affinities to the OMM (Table S1).

Finally, we tested the OMM-FET for detecting small molecule Bcl-2 inhibitors. In addition to ABT-263, we also used HA14-1 (MW = 409.2 g/mol), another Bcl-2 inhibitor with a binding affinity significantly lower than that of ABT-263.⁴²⁻⁴³ When different concentrations of ABT-263 was added onto the OMM-FET, we observed a stepwise decrease of absolute I_{ds} values following each addition (Figure 5C). When the sample was switched to the solution of HA14-1, a similar trend of I_{ds} after each addition was also observed, but with a smaller step than that of ABT-263. Based on these measurements, we also found linear correlations between the changes of I_{ds} and the inhibitor concentrations (Figure 5D). The slope of ABT-263 fitting is significantly larger than that of the HA14-1 fitting, confirming the ability of the OMM-FET to distinguish molecules that bind with the same OMM with different affinities (Table S2).

In summary, we derived the OMM from mouse livers and successfully coated the membrane onto both nanoparticles and FET devices. During the membrane derivation and the

coating processes, membrane surface proteins and their functions were well preserved. The coated OMM showed an orientation consistent with that of the membrane on the intact mitochondria. The OMM-NPs bound with OMM-specific ligands and neutralized their toxicity both in vitro and in vivo. The OMM-FETs were able to detect OMM agonists and differentiate them corresponding to their induced changes in the FET conductance. The coating of OMM onto these substates extends cell membrane coating technology from the plasma membranes of source cells to the intracellular membranes for broader biointerfacing functions. Selective binding of OMM-NPs with mitochondrial ligands may also enable other applications such as immune modulation for immunotherapy. 44 The membranes of other cell organelles, such as nucleus, endoplasmic reticulum, Golgi apparatus, and lysosomes, share the same basic structure as mitochondrial membrane. Therefore, it is anticipated that these cell organelles' membranes can be coated onto synthetic substrates. In our study, the OMM derivation relies on a centrifugation method, which is suitable for large-scale production. As intracellular membranes play a pivotal role in modulating physiological functions within the cells, leveraging them with the cell membrane coating technology is expected to open many new opportunities for future biomedical research and applications.

ASSOCIATED CONTENT

Supporting Information

The Supporting Information is available free of charge at https://pubs.acs.org/doi/xxx.

Materials and methods, Figures S1-S6, and Tables S1 and S2 (PDF)

AUTHOR INFORMATION

15

Corresponding Author:

*Email: w5gao@ucsd.edu. Tel: 858-822-6273

*Email: zhang@ucsd.edu. Tel: 858-246-0999

ORCID

Weiwei Gao: 0000-0001-5196-4887

Liangfang Zhang: 0000-0003-0637-0654

Author Contributions

L.Z. W.G., Q.Z. and H.G. conceived the idea and designed the experiments. H.G., Q.Z, A.K,

Y.D., Z.Z., and F.C. performed all experiments. All authors analyzed and discussed the data.

H.G., Q.Z., S.X., W.G., and L.Z. wrote the paper.

Notes

The authors declare no competing financial interest.

ACKNOWLEDGEMENTS

This work is supported by the Defense Threat Reduction Agency Joint Science and Technology

Office for Chemical and Biological Defense under Grant Number HDTRA1-21-1-0010 and the

National Science Foundation Grant DMR-1904702.

REFERENCES

Fang, R. H.; Kroll, A. V.; Gao, W.; Zhang, L.; Cell membrane coating nanotechnology.

Adv. Mater. 2018, 30, 1706759.

(2) Hu, C. M. J.; Fang, R. H.; Wang, K. C.; Luk, B. T.; Thamphiwatana, S.; Dehaini, D.;

Nguyen, P.; Angsantikul, P.; Wen, C. H.; Kroll, A. V.; Carpenter, C.; Ramesh, M.; Qu, V.;

16

- Patel, S. H.; Zhu, J.; Shi, W.; Hofman, F. M.; Chen, T. C.; Gao, W.; Zhang, K.; Chien, S.; Zhang, L.; Nanoparticle biointerfacing by platelet membrane cloaking. *Nature* **2015**, *526*, 118-121.
- (3) Hu, C. M. J.; Fang, R. H.; Luk, B. T.; Chen, K. N. H.; Carpenter, C.; Gao, W.; Zhang, K.; Zhang, L.; 'Marker-of-self' functionalization of nanoscale particles through a top-down cellular membrane coating approach. *Nanoscale* **2013**, *5*, 2664-2668.
- (4) Zhang, Q. Z.; Dehaini, D.; Zhang, Y.; Zhou, J. L.; Chen, X. Y.; Zhang, L.; Fang, R. H.; Gao, W.; Zhang, L.; Neutrophil membrane-coated nanoparticles inhibit synovial inflammation and alleviate joint damage in inflammatory arthritis. *Nat. Nanotechnol.* 2018, 13, 1182-1190.
- (5) Hu, C. M. J.; Fang, R. H.; Copp, J.; Luk, B. T.; Zhang, L.; A biomimetic nanosponge that absorbs pore-forming toxins. *Nat. Nanotechnol.* **2013**, *8*, 336-340.
- (6) Hu, C. M. J.; Fang, R. H.; Luk, B. T.; Zhang, L.; Nanoparticle-detained toxins for safe and effective vaccination. *Nat. Nanotechnol.* **2013**, *8*, 933-938.
- (7) Wei, X. L.; Ran, D. N.; Campeau, A.; Xiao, C.; Zhou, J. R.; Dehaini, D.; Jiang, Y.; Kroll, A. V.; Zhang, Q. Z.; Gao, W.; Gonzalez, D. J.; Fang, R. H.; Zhang, L.; Multiantigenic nanotoxoids for antivirulence vaccination against antibiotic-resistant gram-negative bacteria. *Nano Lett.* 2019, 19, 4760-4769.
- (8) Gong, H.; Chen, F.; Huang, Z. L.; Gu, Y.; Zhang, Q. Z.; Chen, Y. J.; Zhang, Y.; Zhuang, J.; Cho, Y. K.; Fang, R. N. H.; Gao, W.; Xu, S.; Zhang, L.; Biomembrane-modified field effect transistors for sensitive and quantitative detection of biological toxins and pathogens. ACS Nano 2019, 13, 3714-3722.

- (9) Hu, C. M. J.; Zhang, L.; Aryal, S.; Cheung, C.; Fang, R. H.; Zhang, L.; Erythrocyte membrane-camouflaged polymeric nanoparticles as a biomimetic delivery platform. *Proc. Natl. Acad. Sci. U. S. A.* **2011,** *108*, 10980-10985.
- (10) Wang, S.; Duan, Y.; Zhang, Q.; Komarla, A.; Gong, H.; Gao, W.; Zhang, L.; Drug targeting *via* platelet membrane–coated nanoparticles. *Small Structures* **2020**, *1*, 2000018
- (11) Fang, R. H.; Hu, C. M. J.; Luk, B. T.; Gao, W.; Copp, J. A.; Tai, Y. Y.; O'Connor, D. E.; Zhang, L.; Cancer cell membrane-coated nanoparticles for anticancer vaccination and drug delivery. *Nano Lett.* **2014**, *14*, 2181-2188.
- (12) Thamphiwatana, S.; Angsantikul, P.; Escajadillo, T.; Zhang, Q. Z.; Olson, J.; Luk, B. T.; Zhang, S.; Fang, R. H.; Gao, W.; Nizet, V.; Zhang, L.; Macrophage-like nanoparticles concurrently absorbing endotoxins and proinflammatory cytokines for sepsis management. *Proc. Natl. Acad. Sci. U. S. A.* **2017**, *114*, 11488-11493.
- (13) Gao, C. Y.; Lin, Z. H.; Jurado-Sanchez, B.; Lin, X. K.; Wu, Z. G.; He, Q.; Stem cell membrane-coated nanogels for highly efficient *in vivo* tumor targeted drug delivery. *Small* **2016**, *12*, 4056-4062.
- (14) Angsantikul, P.; Thamphiwatana, S.; Zhang, Q. Z.; Spiekermann, K.; Zhuang, J.; Fang, R. H.; Gao, W.; Obonyo, M.; Zhang, L.; Coating nanoparticles with gastric epithelial cell membrane for targeted antibiotic delivery against helicobacter pylori infection. *Adv. Ther.* 2018, 1, 1800016.
- (15) Gao, W.; Fang, R. H.; Thamphiwatana, S.; Luk, B. T.; Li, J. M.; Angsantikul, P.; Zhang, Q. Z.; Hu, C. M. J.; Zhang, L.; Modulating antibacterial immunity via bacterial membrane-coated nanoparticles. *Nano Lett.* 2015, 15, 1403-1409.

- (16) Xiong, F.; Ling, X.; Chen, X.; Chen, J.; Tan, J. X.; Cao, W. J.; Ge, L.; Ma, M. L.; Wu, J.; Pursuing specific chemotherapy of orthotopic breast cancer with lung metastasis from docking nanoparticles driven by bioinspired exosomes. *Nano Lett.* **2019**, *19*, 3256-3266.
- (17) Zhang, Y.; Chen, Y. J.; Lo, C.; Zhuang, J.; Angsantikul, P.; Zhang, Q. Z.; Wei, X. L.; Zhou, Z. D.; Obonyo, M.; Fang, R. H.; Gao, W.; Zhang, L.; Inhibition of pathogen adhesion by bacterial outer membrane-coated nanoparticles. *Angew. Chem. Int. Ed.* 2019, 58, 11404-11408.
- (18) Kroll, A. V.; Fang, R. H.; Zhang, L.; Biointerfacing and applications of cell membrane-coated nanoparticles. *Bioconj. Chem.* **2017**, *28*, 23-32.
- (19) Mouritsen, O. G.; Bloom, M.; Mattress model of lipid-protein interactions in membranes. *Biophys. J.* **1984**, *46*, 141-153.
- (20) Klymchenko, A. S.; Kreder, R.; Fluorescent probes for lipid rafts: From model membranes to living cells. *Chem. Biol.* **2014**, *21*, 97-113.
- (21) Yao, J.; Fan, Y.; Li, Y. K.; Huang, L.; Strategies on the nuclear-targeted delivery of genes. *J. Drug Targeting* **2013**, *21*, 926-939.
- (22) Selvi, B. R.; Jagadeesan, D.; Suma, B. S.; Nagashankar, G.; Arif, M.; Balasubramanyam, K.; Eswaramoorthy, M.; Kundu, T. K.; Intrinsically fluorescent carbon nanospheres as a nuclear targeting vector: Delivery of membrane-impermeable molecule to modulate gene expression *in vivo*. *Nano Lett.* **2008**, *8*, 3182-3188.
- (23) Nurunnabi, M.; Khatun, Z.; Badruddoza, A. M.; McCarthy, J. R.; Lee, Y. K.; Huh, K. M.; Biomaterials and bioengineering approaches for mitochondria and nuclear targeting drug delivery. *ACS Biomater. Sci. Eng.* **2019**, *5*, 1645-1660.

- (24) Serrano-Puebla, A.; Boya, P.; Lysosomal membrane permeabilization as a cell death mechanism in cancer cells. *Biochem. Soc. Trans.* **2018**, *46*, 207-215.
- (25) Miller, S.; Krijnse-Locker, J.; Modification of intracellular membrane structures for virus replication. *Nat. Rev. Microbiol.* **2008**, *6*, 363-374.
- (26) Burmann, F.; Ebert, N.; van Baarle, S.; Bramkamp, M.; A bacterial dynamin-like protein mediating nucleotide-independent membrane fusion. *Mol. Microbiol.* **2011,** *79*, 1294-1304.
- (27) Frezza, C.; Cipolat, S.; Scorrano, L.; Organelle isolation: Functional mitochondria from mouse liver, muscle and cultured filroblasts. *Nat. Protoc.* **2007,** *2*, 287-295.
- (28) Waite, M.; Isolation of rat liver mitochondrial membrane fractions and localization of phospholipase a. *Biochemistry* **1969**, *8*, 2536-2542.
- (29) Luk, B. T.; Hu, C. M. J.; Fang, R. N. H.; Dehaini, D.; Carpenter, C.; Gao, W.; Zhang, L.; Interfacial interactions between natural rbc membranes and synthetic polymeric nanoparticles. *Nanoscale* **2014**, *6*, 2730-2737.
- (30) Perkins, G.; Renken, C.; Martone, M. E.; Young, S. J.; Ellisman, M.; Electron tomography of neuronal mitochondria: Three-dimensional structure and organization of cristae and membrane contacts. *J. Struct. Biol.* **1997**, *119*, 260-272.
- (31) Depierre, J. W.; Ernster, L.; Enzyme topology of intracellular membranes. *Annu. Rev. Biochem.* **1977,** *46*, 201-262.
- (32) Blobel, G.; Intracellular protein topogenesis. *Proc. Natl. Acad. Sci. U. S. A.* **1980,** 77, 1496-1500.
- (33) Wendt, M. D.; Discovery of ABT-263, a Bcl-family protein inhibitor: Observations on targeting a large protein-protein interaction. *Expert Opin. Drug Discov.* **2008**, *3*, 1123-1143.

- (34) Riddy, D. M.; Goy, E.; Delerive, P.; Summers, R. J.; Sexton, P. M.; Langmead, C. J.; Comparative genotypic and phenotypic analysis of human peripheral blood monocytes and surrogate monocyte-like cell lines commonly used in metabolic disease research. *PLoS One* **2018**, *13*, e0197177.
- (35) Vogler, M.; Hamali, H. A.; Sun, X. M.; Bampton, E. T. W.; Dinsdale, D.; Snowden, R. T.; Dyer, M. J. S.; Goodall, A. H.; Cohen, G. M.; Bcl2/Bcl-x-l inhibition induces apoptosis, disrupts cellular calcium homeostasis, and prevents platelet activation. *Blood* **2011**, *117*, 7145-7154.
- (36) Lin, Q. H.; Que, F. C.; Gu, C. P.; Zhong, D. S.; Zhou, D.; Kong, Y.; Yu, L.; Liu, S. W.; Abt-263 induces G(1)/G(0)-phase arrest, apoptosis and autophagy in human esophageal cancer cells *in vitro*. *Acta Pharmacol*. *Sin*. **2017**, *38*, 1632-1641.
- (37) Schoenwaelder, S. M.; Jarman, K. E.; Gardiner, E. E.; Hua, M.; Qiao, J. L.; White, M. J.; Josefsson, E. C.; Alwis, I.; Ono, A.; Willcox, A.; Andrews, R. K.; Mason, K. D.; Salem, H. H.; Huang, D. C. S.; Kile, B. T.; Roberts, A. W.; Jackson, S. P.; Bcl-xL-inhibitory BH3 mimetics can induce a transient thrombocytopathy that undermines the hemostatic function of platelets. *Blood* 2011, *118*, 1663-1674.
- (38) Kaefer, A.; Yang, J. N.; Noertersheuser, P.; Mensing, S.; Humerickhouse, R.; Awni, W.; Xiong, H.; Mechanism-based pharmacokinetic/pharmacodynamic meta-analysis of navitoclax (ABT-263) induced thrombocytopenia. *Cancer Chemother. Pharmacol.* **2014**, 74, 593-602.
- (39) Lin, T. W.; Hsieh, P. J.; Lin, C. L.; Fang, Y. Y.; Yang, J. X.; Tsai, C. C.; Chiang, P. L.; Pan, C. Y.; Chen, Y. T.; Label-free detection of protein-protein interactions using a

- calmodulin-modified nanowire transistor. *Proc. Natl. Acad. Sci. U. S. A.* **2010,** *107*, 1047-1052.
- (40) Hwang, M. T.; Landon, P. B.; Lee, J.; Choi, D.; Mo, A. H.; Glinsky, G.; Lal, R.; Highly specific snp detection using 2D graphene electronics and DNA strand displacement. *Proc. Natl. Acad. Sci. U. S. A.* **2016**, *113*, 7088-7093.
- (41) Gruner, G.; Carbon nanotube transistors for biosensing applications. *Anal. Bioanal. Chem.* **2006,** *384*, 322-335.
- (42) Wang, J. L.; Liu, D. X.; Zhang, Z. J.; Shan, S. M.; Han, X. B.; Srinivasula, S. M.; Croce, C. M.; Alnemri, E. S.; Huang, Z. W.; Structure-based discovery of an organic compound that binds Bcl-2 protein and induces apoptosis of tumor cells. *Proc. Natl. Acad. Sci. U. S. A.* 2000, 97, 7124-7129.
- (43) Vogler, M.; Dinsdale, D.; Dyer, M. J. S.; Cohen, G. M.; Bcl-2 inhibitors: Small molecules with a big impact on cancer therapy. *Cell Death Differ.* **2009**, *16*, 360-367.
- (44) Zeng, Z. L.; Pu, K. Y.; Improving cancer immunotherapy by cell membrane-camouflaged nanoparticles. *Adv. Funct. Mater.* **2020,** *30*, 2004397.

Table of Contents (TOC) Graphic

